Nanoscale

Accepted Manuscript

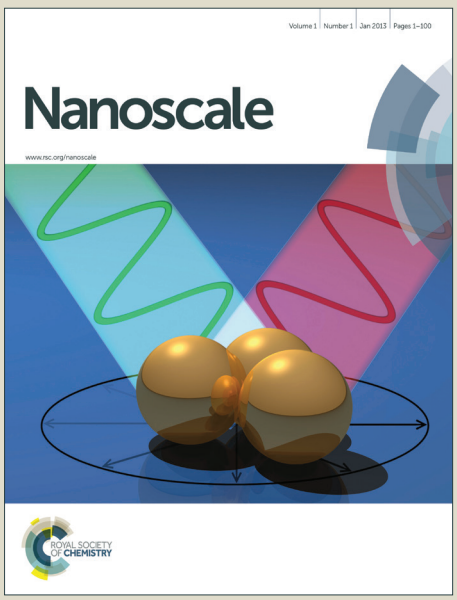

ROYAL SOCIETY OF CHEMISTRY

www.rsc.org/nanoscale

Journal Name

RSCPublishing

ARTICLE

Two dimensional dipolar coupling in monolayers of silver and gold nanoparticles on a dielectric substrate

Cite this: DOI: 10.1039/xoxxoooooox

*Yu Liu, Sylvie Begin-Colin, Benoît P. Pichon, Cedric Leuvrey, Dris Ihiawakrim, Mircea Rastei, Guy Schmerber, Mircea Vomir, Jean Yves Bigot**

Received ooth January 2012,
Accepted ooth January 2012

DOI: 10.1039/xoxxoooooox

www.rsc.org/

The dimensionality of assembled nanoparticles plays an important role in their optical and magnetic properties, via dipolar effects and the interaction with their environment. In this work we develop a methodology for distinguishing between two (2D) and three (3D) dimensional collective interactions on the surface plasmon resonance of assembled metal nanoparticles. Towards that goal, we elaborate different sets of Au and Ag nanoparticles as suspensions, random 3D arrangements and well organized 2D arrays. Then we model their scattering cross section using effective field methods in dimension *n*, including interparticle as well as particle/substrate dipolar interactions. For this modelling, two effective field medium approaches are employed, taking into account the filling factors of the assemblies. Our results are important for realizing photonics amplifier devices.

Introduction

Metal nanoparticles (NPs) are widely used in plasmonics[1], surface enhanced scattering[2], bio-imaging[3], nanomedicine[4] and quantum optics[5], because of their resonant optical properties due to surface plasmons (SP), resulting from the competition between the enhanced local field and the long range interparticle dipolar interactions[6,7]. The spectral position of the surface plasmon (SP) resonance of NPs is known[8] to depend mainly on the size, the shape, the interparticle distances and the dielectric constant of the surrounding medium (nature of ligands, solvents and substrate) [9,10]. The notion of effective medium becomes then essential[6]. For several applications in photonics or microelectronics, a key feature is that the peculiarities of the SP (spectral position, width, amplitude) must be kept stable on a large scale, therefore involving dense assemblies of such nanoparticles. Ideally, one should aim at making 2D arrangements that can be easily cast into a monolayer on any type of substrate. In that context, besides controlling the SP for such monolayer on substrate, understanding of the dipolar effects associated to the interparticle interactions is very important[11], in particular for predicting the 2D versus 3D behavior of the resonant plasmonic properties. In this work, we explore these effects of dimensionality on the SP's elaborating Au and Ag NP monolayers by using the Langmuir-Blodgett (LB) technique[12], and by analyzing their SP properties by comparison with the ones of the same NPs in suspensions or drop casting forms. The modeling, performed within the effective field medium (EFM) approximation[13], in addition to

strongly underlining the 2D character of the SP in our LB-monolayers as well as the importance of the filling factor, allows obtaining very good numerical fits for all types of NPs assemblies.

Regarding interacting clusters, following the intensive works performed in the 70ies on metallic islands and ellipsoidal inclusions[14,15,16], recent works have focused on large dots with various shapes[17,18], Dimers of Au dots[19] or chains of NPs[20] by discrete dipole approximation (DDA)[21]. For example, it has been demonstrated that the near-field coupling between 88 nm Au nanodisc pairs decreases with the interparticle separation (edge-to-edge)[22]. Furthermore, the 3D assembling of plasmonic clusters has been reported and modelled by a finite element method to calculate their scattering properties[23]. Despite numerous works describing interacting nanoparticles[24,25], it remains a challenge to distinguish between the 2D versus 3D effects occurring in NP assemblies, made from bottom-up techniques, and to provide accurate fittings of the SP resonances. This is particularly true for monolayers for which the role of the substrate should also be considered in addition to the interparticle dipolar interactions.

Experimental Section

Synthesis of oleylamine capped Au and Ag Nanoparticles

Au NPs: $HAuCl_4.4H_2O$ (50 mg) with oleylamine (OLM) (5 mL) were dissolved in toluene (5 mL) in a flask (100 mL)and refluxed at 110 °C under argon for 3 hours. The as obtained NPs were purified three times by adding ethanol and by centrifugation (8000 rpm during 10 min). After purification, the NPs were easily suspended in chloroform solvent.

Ag NPs: $AgNO_3$ (100 mg) were dissolved in dioctylether (10 mL) with oleylamine (10 mL) as a reducer, the mixture solution was at first maintained at 60°C for 1 h to dissolve the reactants. Then the mixture was heated up to 190 °C under Ar for 2 h. The as prepared NPs have been purified once by adding ethanol and by centrifugation (8000 rpm during 10 min). Thus the size distribution was narrowed (7%) by performing a supplementary digestive ripening step (Figure S1). After the purification step, the NPs were re-suspended in 8 mL oleylamine and toluene (10 mL) and the mixture was heated at reflux for 3h. The as obtained silver NPs were purified only one time before performing the Langmuir Blodgett assembly.

Film preparation

Langmuir Blodgett technique: The used substrate was soaked at room temperature in a Piranha solution (3 : 1 = H_2SO_4:H_2O_2) for 10 min, thoroughly rinsed with H_2O and dried before deposition. Briefly, a small volume (150–200 µl) of a 5 $mg.mL^{-1}$ NPs suspension in chloroform was spread on the water sub-phase of the Langmuir trough (KSV 5000, 576 x 150 mm^2) at room temperature. After stabilization for 10 min, the area available to the NPs is reduced by controlled compressing of the barriers (compression rate: 5 mm per min), and the surface pressure–area isotherm is recorded during the film compression using a Wilhelmy plate. The pressure is stabilized for 10 min at 30 $mN\ m^{-1}$. At this pressure, the film reaches its maximum in density and can be then transferred onto an optical glass (5 cm x 5 cm) or a silicon substrate depending on the characterization. The transfer occurs by the concomitant pulling out of the substrate from the water sub-phase at a rate of 1 mm per min and by moving the barriers with the aim of maintaining the surface pressure at 30 mN. M^{-1} at the air–water interface.

Thermal treatment The LB monolayer was exposed to a thermal treatment at 300°C for 4 h (heating rate of 5 °C per min). Au NPs and Ag NPs LB films were annealed respectively under air and argon atmospheres.

Drop casting the 2D LB films have been compared with the drop casting deposition considered as a self-assembly process. The drop casted film was prepared by evaporating a droplet of 5 $mg.mL^{-1}$ NPs suspension in chloroform onto a glass or silicon substrate under air with a glass cover. The drop casted films consist in 3D multilayer with discontinuous substrate surface coverage. The experiment has

been reproduced several times without succeeding in obtaining a homogeneous and continuous substrate coverage.

Materials Characterization. The NPs were characterized by transmission electron microscopy TEM with a TOPCON model 002B transmission electron microscope operating at 200 kV. The polydispersity in size was calculated from the size measurements of more than 200 NPs. Dynamic light scattering (DLS) measurements were performed on the suspension of NPs in chloroform using a nano-size MALVERN (nano ZS) apparatus. All the transferred films were also characterized by Scanning Electron Microscopy (SEM) (JEOL 6700F equipped with a field emission gun (FEG) and operating at 3 kV). The image analysis was performed using Digital Micrograph (Gatan) and ImageJ software. UV-visible measurements were performed with a conventional Hitachi UV3000 spectrophotometer. Atomic Force Microscopy (AFM) was performed using a Digital Instrument 3100 microscope coupled to a Nanoscope IIIa recorder. Measurements were done in the tapping mode onto substrates. Collected data were analyzed with WSXM software.

Results and discussion

Synthesis of oleylamine capped Au and Ag Nanoparticles

To ensure an ordered assembling on large scales of metal NPs the elaboration and optimization required: i) the NPs size monodispersity. ii) a colloidal stability in fast evaporating organic solvent iii) the nature and the amount of ligands at the surface of NPs. As established for the LB assembling of iron oxide NPs[26,27], the amount of ligands should be the smallest possible to ensure the formation of a continuous monolayer of NPs and to avoid the formation of Langmuir films of ligands. Finally, the interaction between ligands and the NP surface should be weak and reversible to favor their desorption and the formation of Janus NPs upon deposition at the water–air interface enhancing the interaction of the NP surface with OH groups of substrates. Oleylamine ligands have been thus selected to coat the NPs and one step synthesis process has been optimized from Shen *et al.* [28].TEM images show that the NPs are monodisperse in size with a mean size of 12.6 nm and a 8% polydispersity, i.e. standard deviation, (Figure 1a). The dynamic light scattering (DLS) measurement confirmed a good colloidal stability of NPs in chloroform solvent with a monomodal size distribution centered at 15.2 nm (Figure 1a). This mean hydrodynamic diameter is slightly larger than the mean diameter deduced from TEM images due to the oleylamine surface coating ($\Phi_{DLS} = \Phi_{TEM} + 2\Phi_{ligand}$ with Φ_{ligand}~1.3 nm).

The preparation of monodisperse Ag NPs has involved a two-step process including a modified digestive ripening approach described by Zhang et al.[29] (Figure S1 of the supplementary information (SI). The so obtained silver NPs (Figure S1) were purified only one time before performing the Langmuir Blodgett assembly. Indeed, due to the higher sensitivity of Ag NPs to oxidation and the observation that too much purification steps leads to unstable colloidal suspension, an excess of ligands by comparison with Au NPs was necessary. Statistic count from TEM micrograph showed an average diameter of 13.6 nm with a 7% polydispersity, i.e. standard deviation, (Figure 1 and Figure S1). DLS measurements indicated a mean hydrodynamic diameter of 16.1 nm in agreement with NPs coated with oleylamine (Figure 1b).

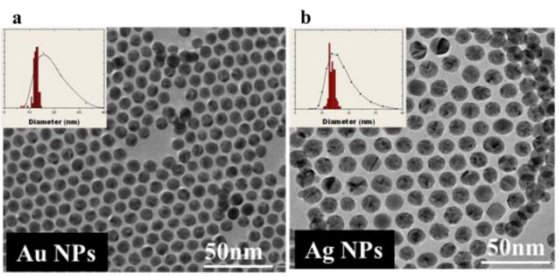

Figure 1. Transmission Electron Microscopy images of Au and Ag nanoparticles. Oleylamine capped. a) 12.6 nm Au NPs. b) 13.6 nm Ag NPs. The insets show the TEM (bar histogram) and dynamic light scattering (continuous curve) size distributions.

Two versus Three dimensional assemblies

Dense 2D arrays over large areas have been further obtained, as shown in Figures 2a) and 2b), using the LB technique[30]. More defects are noticed in the Ag than in the Au LB film. This is easily related to the search of a compromise, for Ag NPs suspension, between the need of a good colloidal stability and also an adequate amount of ligands at the surface of NPs, to prevent them from oxidation considering the low bonding strength of amine with the Ag surface. In this study, an excess of oleylamine ligands was found necessary to provide a good colloidal stability of Ag NPs as indicating from thermogravimetric analysis in SI section 1.

In order to evaluate the degree of ordering in the 2D NPs arrays, image analysis has been performed on the SEM images in figure 2, using Digital Micrograph (Gatan) software[27]. The autocorrelation spectra in LB film have been calculated on a given area (128 x 128 nm^2), and radial profiles have been extracted, which are characteristic of the film structure and of the degree of ordering in the array. The fit of the radial profile allows the deduction of a mean interparticle distance of 13.8 nm for Au film (center to center) and 15.6 nm for Ag film (see Figure S2). Considering the mean TEM diameter of Au NPs and Ag NPs, this fit leads to an average interparticle distance between Au NPs in the 2D monolayer of 1.2 ± 1 nm (edge to edge) and 2 ± 0.95 nm for Ag 2D monolayer. However, it should be noticed that the interparticle distance monolayer is extremely hard to determine with accuracy by using the autocorrelation spectra due to the presence of defects. This result suggests a partial interdigitation of peripheral alkyl chains of molecules between two adjacent NPs as often observed in LB films[26,27]. Determination of the mean interparticle distance from SEM images leads to a mean value (edge to edge) of 2 nm ± 0.5 nm for Au NPs and 2.5 nm ± 0.5 nm for Ag NPs (see Table 1).

A roughness of about 2.2 and 8 nm were measured by Atomic Force Microscopy for Au and Ag LB films respectively (Figures S3a and S3c in SI). It confirms the formation of extremely close packed Au NPs while for the Ag films the larger interparticle distances (ID), due to the excess of ligands in suspension, results in an average larger rugosity.The corresponding filling factors f are: $f_{LB}^{(Au)} = 0.67$ and $f_{LB}^{(Ag)} = 0.60$.

Multilayer 3D films have also been obtained by drop casting (Figures 2c, 2d) and in Figures S3b) and S3d) in SI, by adjusting the NPs suspension concentration and the evaporation velocity although, discontinuous NP assemblies were related to the deposition method itself. The filling factors are: $f_{drop\_cast}^{(Au)} = 0.41$ and $f_{drop\_cast}^{(Ag)} = 0.20$.

Finally, thermal treatments of the Au monolayer resulted in films of collapsed 20 ± 3 nm Au NPs with an average ID of 9.5 ±2 nm corresponding to a factor $f_{LB\_anneal}^{(Au)} = 0.41$ (Figure 2e and Table 1). The ligands were removed under air environment at 300°C. However, as small dimers or trimers closer to one another are noticeable, the notion of filling factor is questionable in that case. A similar heat treatment on Ag LB under an Ar atmosphere, to avoid oxidation, led to 2D films with larger Ag particle sizes (≥ 50 nm) and larger ID (> 150 nm) (Figure 2f and Table 1). The corresponding effective filling factor is: $f_{LB\_anneal}^{(Ag)} = 0.06$. Note also the existence of clustering which is favored by higher coalescence rate of Ag NPs because of the lower melting point, the larger diffusion coefficient and the weaker ligand interaction for Ag in comparison with gold[31].

The UV visible spectra of all NP assemblies show the shift of all SP resonances in comparison to isolated NPs in suspension with the following trend: $\lambda_{suspension} < \lambda_{monolayer}$ annealing $< \lambda_{drop\ casting} < \lambda_{monolayer}$ for both Au and Ag NPs (Figure 3a, 3b). In the following,

we account for this trend, considering interacting nanoparticles with different filling factors in 2D or 3D, using EFM approaches.

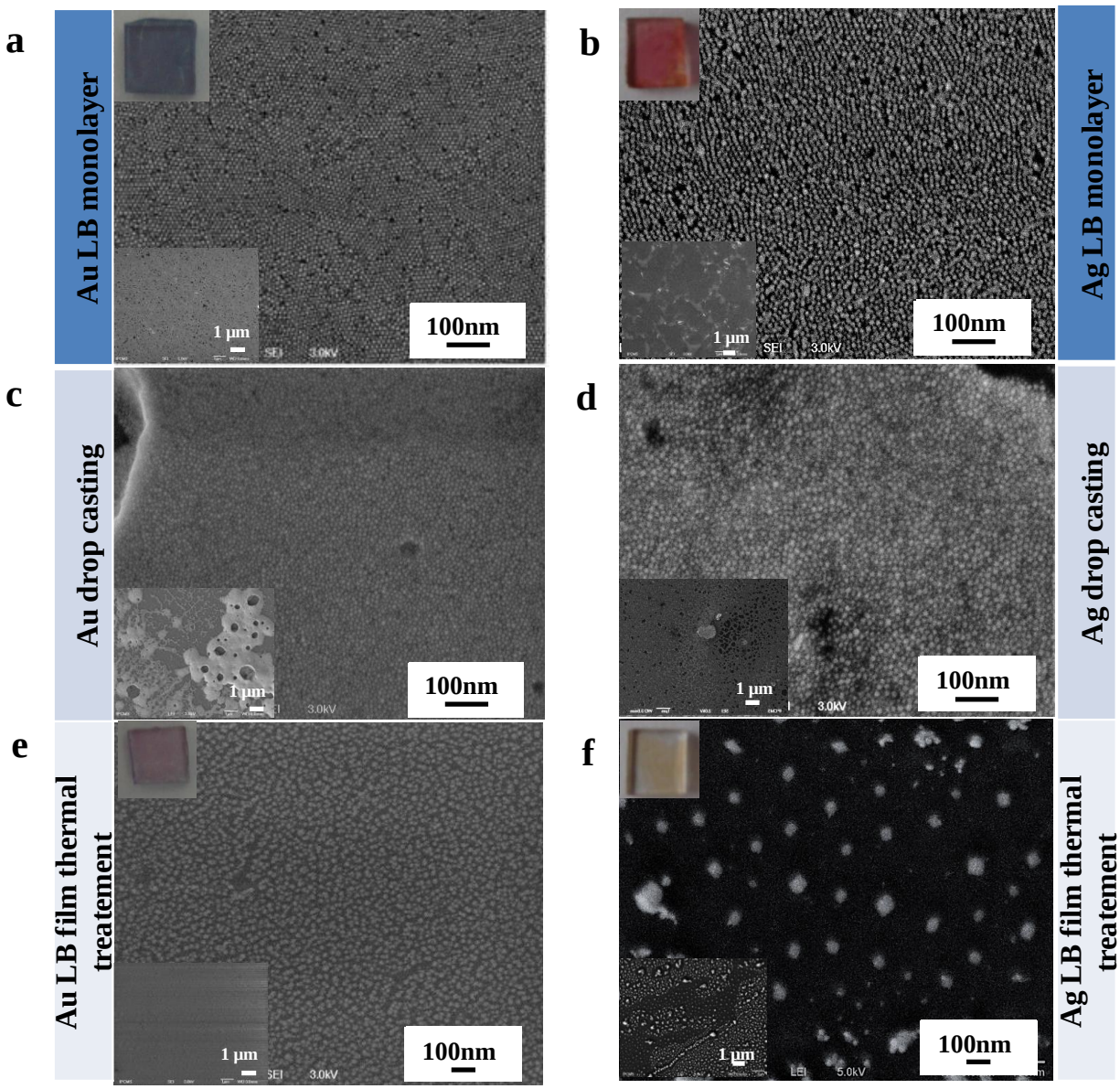

Figure 2. Scanning Electron Microscopy images and optical absorption of NPs films. a) Dense hexagonal packed 12.6 nm Au NPs 2D LB arrays over large area. Inset: top: optical image shows the blue colored Au film on glass substrate; down: large scale SEM image with 1 µm magnification). b) 13.6 nm Ag NPs LB films. Inset: top: red colored Ag film on glass substrate; down: 1 µm magnification. c) Au multilayer and d) Ag multilayer prepared by droplet deposition and auto-assembling triggered by solvent evaporation. Inset : down: 1 µm magnification. e) Au LB film and f) Ag LB film after thermal annealing. Inset: pink colored Au film (top e) and light yellow colored Ag film (top f) on glass substrate and 1 µm magnification (down)).

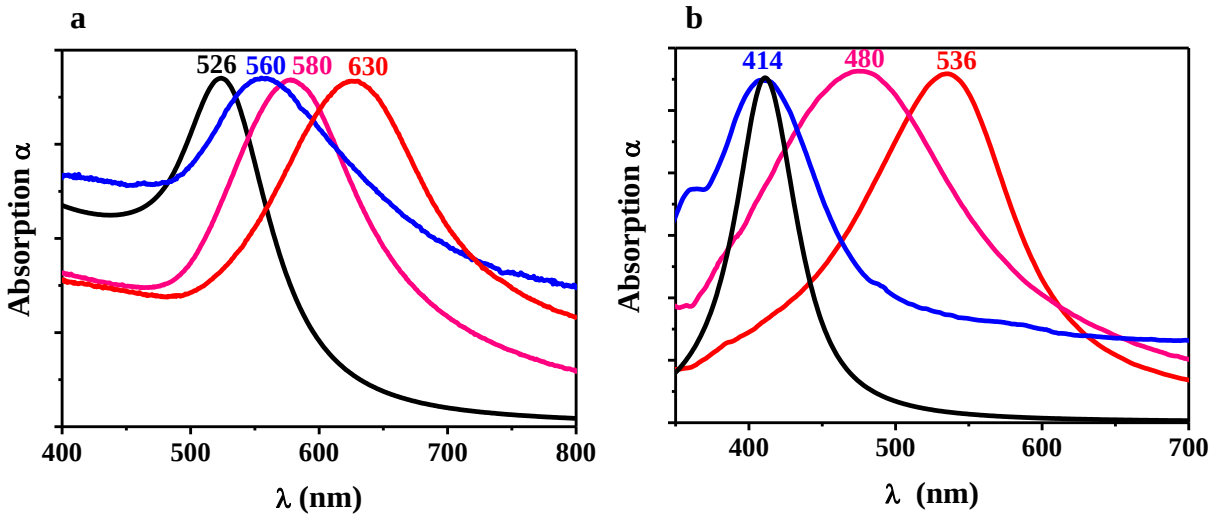

Figure 3. a) and b): Surface plasmon resonance of the various NPs in the UV-Visible spectral region. Au (g) and Ag (h) films on glass substrate. Black line: NPs suspension. Blue line: thermal annealing film. Pink line: drop casting film. Red line: LB film.

Au / Ag	Monolayer (nm)	Drop casting (nm)	Monolayer annealing (nm)
Δλ SPR shift	104 / 122	54 / 62	34 / 6
NPs size	12.6 / 13.6	12.6 / 13.6	~ 20 / > 50
Interparticles distance (id)	~2 / ~2.5	~ 1.9 * / ~3 *	~ 9.5 / >150
Theoretical id	1.2 / 2	-	-

*The interparticles distance for drop casting films was considered equivalent with those measured from self-assembled NPs in TEM images.

Table 1. Wavelength absorption shift (Δλ) relative to the one of Au NPs in suspension and variation of interparticles distances obtained from SEM images for the different assemblies.

Modeling of the optical response of nanoparticle assemblies

The modelling of the 2D versus 3D dipolar effects have been made by two different EFM approaches. First we combine Maxwell Garnett (MG) and Bruggeman (BRUG) theories in dimension n which, as discussed below, we found to be a good compromise for taking into account both short range (local field) and long range (dipole-dipole interaction) dipolar effects. Second, in the 2D case, we considered the interaction of NPs on a substrate, using the dipole image modelling previously developed for small metallic islands[10]. For both approaches we start by modeling the complex bulk dielectric functions of Au and Ag (see details in section 2a of the SI). The real and imaginary parts of $\tilde{\varepsilon}$ are shown in figures S4a)-SI-4d) of SI with the corresponding fit parameters given in the table S1 of the SI.

Effective medium approach without and with nanoparticle interaction

For modelling the NPs films we consider first isolated NPs in suspension (see details in section 2b of SI) using the 3D MG model. This allows us obtaining the main parameters of the "non-interacting" NPs (values in Table S2 of SI), like the damping of the free electrons $\hbar\gamma$ which is slightly larger in the NPs as compared to the bulk (aV_F / R term discussed in SI) and the interband damping $\hbar\alpha$ which increases due to surface induced electron-electron

scattering (taken into account in the W_{ee} coefficient of equation (S2) in SI). The corresponding fits of the absorption for the Au and Ag isolated nanoparticles are shown in figures 4a) and 4b).

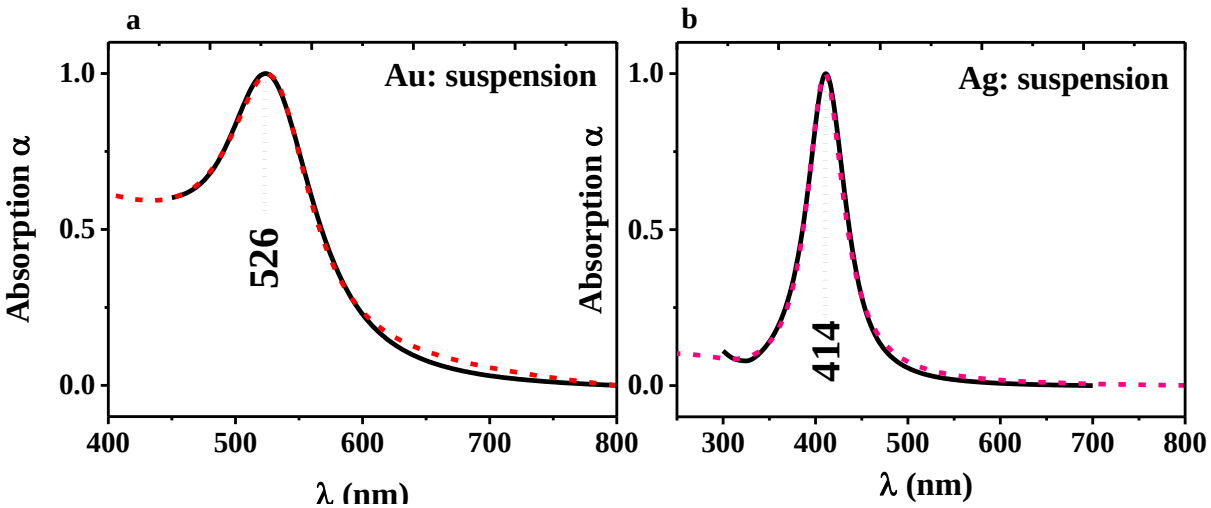

Figure 4. Fits of Au and Ag nanoparticles using MG models. Red dashed line: model, black line experiment. a) Au and b) Ag suspensions.

To take into account the effects of interparticles interaction for the films, we then use the effective model of Bruggeman (dielectric function $\tilde{\varepsilon}_{Brug}$)[32]:

$$f\frac{\tilde{\varepsilon}-\tilde{\varepsilon}_{Brug}}{\tilde{\varepsilon}+(n-1)\tilde{\varepsilon}_{Brug}}+(1-f)\frac{\tilde{\varepsilon}_0-\tilde{\varepsilon}_{Brug}}{\tilde{\varepsilon}_0+(n-1)\tilde{\varepsilon}_{Brug}}=0 \quad (1)$$

For large filling factors f like the ones of the 2D monolayer and 3D drop-casting films, the Bruggeman dielectric function alone overestimates the long range interaction. Implicitly Bruggeman theory considers that there is a constant dipolar field. As a consequence the contribution of the interacting NPs to the red and IR absorption spectra is far too important. This is shown in Figure 5 where the absorption spectra of the Au SP resonances in the 2D BRUG (5a) and 3D BRUG (Figure 5b) models, using equation (1) for increasing filling factors f. Clearly the maximum of the SP resonances rapidly shifts to the infra-red spectrum for filling factors which are still much lower than the experimental one (0.67 for the LB Au monolayer). This is shown by the dashed lines in both figures. The fact that it diverges faster for the 3D case than 2D one is due to the larger "mean field" dipolar interaction which is intrinsic to the representative Bruggeman elementary cell considered in the Effective Field Medium theory. One can also see that, for low filling factors, the dashed lines converge towards values close to 500 nm or 530 nm which are the corresponding 2D or 3D MG cases of isolated NPs.

Journal Name RSCPublishing

ARTICLE

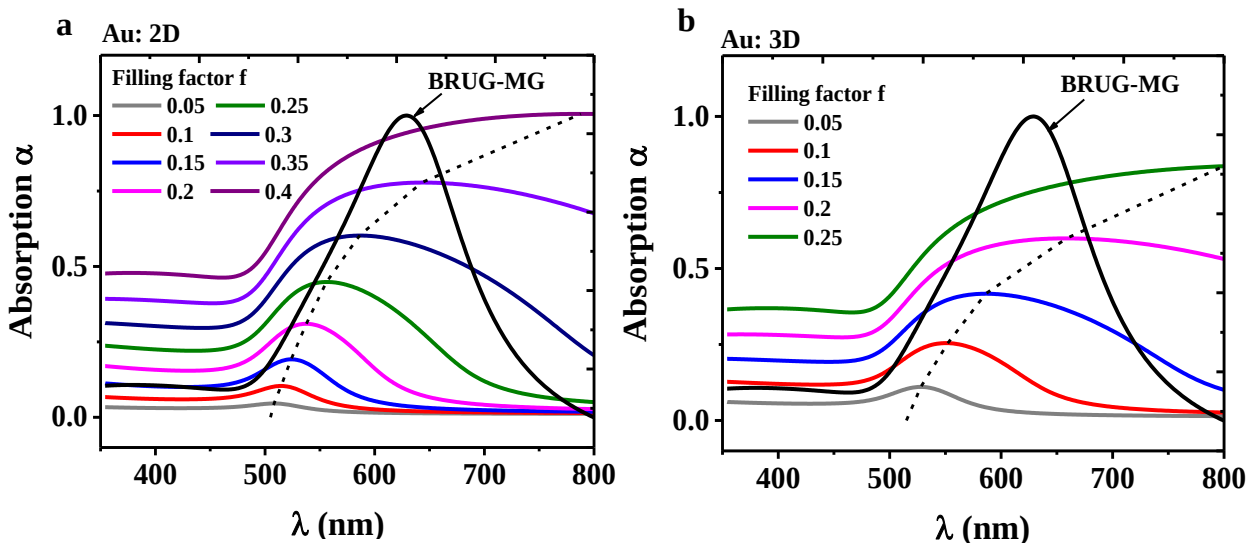

Figure 5: Absorption spectra of Au NPs calculated with the Bruggeman model for different filling factors. a) 2D case and b) 3D case. The 2D theoretical fit is represented in black. The dashed line represents the spectral position of the maximum of the Surface Plasmon.

Instead, we found that the combination of BRUG and MG models provides a better match than BRUG only. The corresponding dielectric function $\tilde{\varepsilon}_{BRUG-MG}$ which we use for a dimensionality n is given by equation (1) in which the dielectric function $\tilde{\varepsilon}$ is replaced by $\tilde{\varepsilon}_{MG}$. The parameters that we have used are summarized in Table 2.

Au films of NPs	dimension n	$\hbar\gamma$ (eV)	$\hbar\alpha_0$ (eV)	W_{ee} (eV^{-1})	f	$\Re(\tilde{n}_0)$	$\Im(\tilde{n}_0)$
LB monolayer	2	0.18	0.25	0.5	0.67	1.53	0.01
Drop casting	3	0.18	0.25	0.5	0.4	1.53	0.01
Annealed monolayer	2	0.18	0.25	0.5	0.54	1.53	0.01

Ag films of NPs	dimension n	$\hbar\gamma$ (eV)	$\hbar\alpha_0$ (eV)	W_{ee} (eV^{-1})	f	$\Re(\tilde{n}_0)$	$\Im(\tilde{n}_0)$
LB monolayer	2	0.28	0.4	0.3	0.6	1.53	0.01
Drop casting	3	0.28	0.4	0.3	0.2	1.53	0.01
Annealed monolayer	2	0.28	0.4	0.3	0.36	1.53	0.01

Table 2. Parameters used for fitting the absorption of the various assemblies of Au and Ag nanoparticles. n : dimension of the system; $\hbar\gamma$: Drude d□dude ; $\hbar\alpha_0$: interband damping constant; W_{ee}: electron-electron scattering cross section ; f : filling factor ; $\Re(\tilde{n}_0)$ (resp. $\Im(\tilde{n}_0)$) real and imaginary part of surrounding medium refractive index.

Journal Name RSCPublishing

ARTICLE

Figures 6a) (for Au) and 6b) (for Ag) show the absorption of the 2D monolayers while figures 6c) (for Au) and 6d) (for Ag) show the fits for the 3D case of the drop casting films. In addition, figures 6e) (for Au) and 6f) (for Ag) corresponds to the fit of the 2D monolayers using BRUG-MG after thermal treatment. The filling factor used in the fit are however larger $f_{LB\_anneal}^{(Au)}(\text{BRUG}-\text{MG}) = 0.56$ and $f_{LB\_anneal}^{(Ag)}(\text{BRUG}-\text{MG}) = 0.36$ instead of the 0.4 and 0.06 experimental ones. This is due to an underestimation of the experimental filling factors because, as discussed above, obviously there are several dimers and trimers in the SEM images (see figures 2e) and 2f)). This is most obvious for the case of Ag where the clustering is very important.

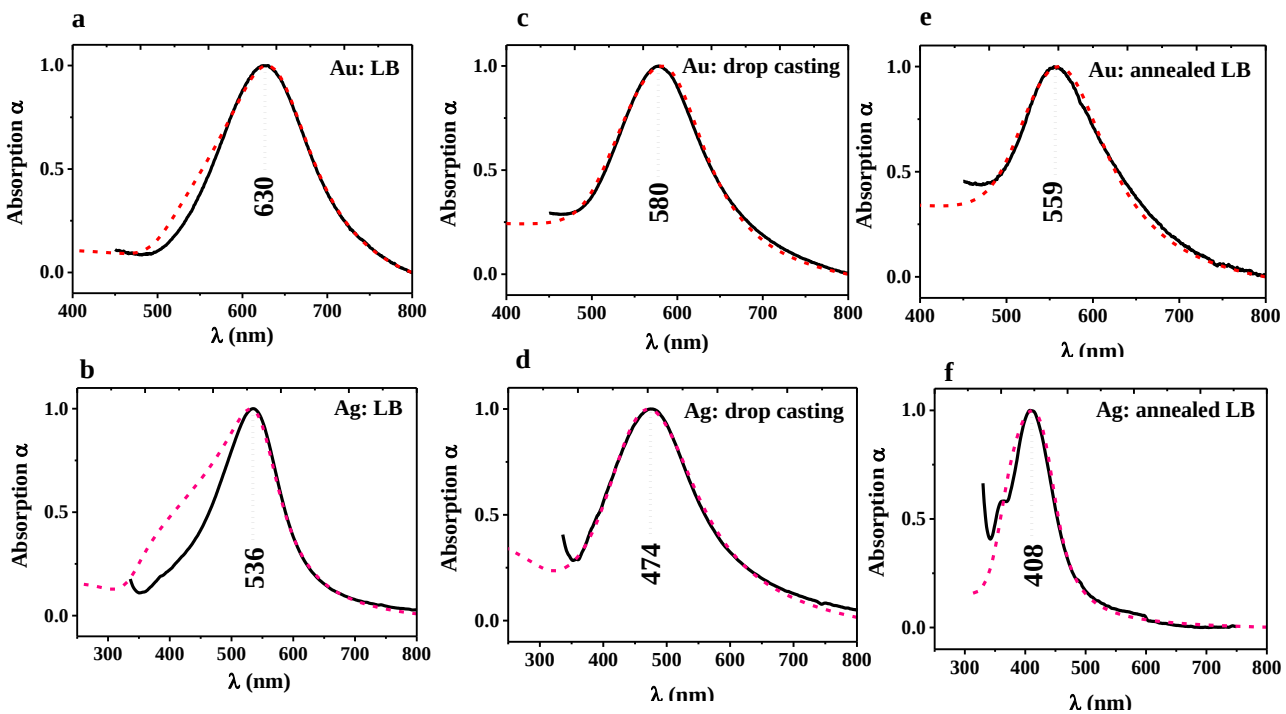

Figure 6. Fits of Au and Ag nanoparticles using BRUG-MG models. Red dashed line: model, black line experiment. a) Au and b) Ag LB monolayers; c) Au and d) Ag drop casting films; e) Au and f) Ag annealed LB monolayers. The fits parameters are in Table 2.

The importance of the system dimensionality is crucial. This is exemplified in figure 7 which shows the position of the surface plasmon resonance λ_{SP} for the 2D and 3D cases as a function of the filling factor f for Au (Figures 7a and 7c) and for Ag (Figures 7 b and 7d). As shown by the dotted lines in figures 7c) and 7d) clearly, for the experimentally observed filling factors $f_{LB}^{(Au)} = 0.67$ and $f_{LB}^{(Ag)} = 0.60$, the monolayers can only be fitted with $n = 2$ and the drop casting with $n = 3$ ($f_{drop\_cast}^{(Au)} = 0.41$ and $f_{drop\_cast}^{(Ag)} = 0.20$).

Journal Name RSCPublishing

ARTICLE

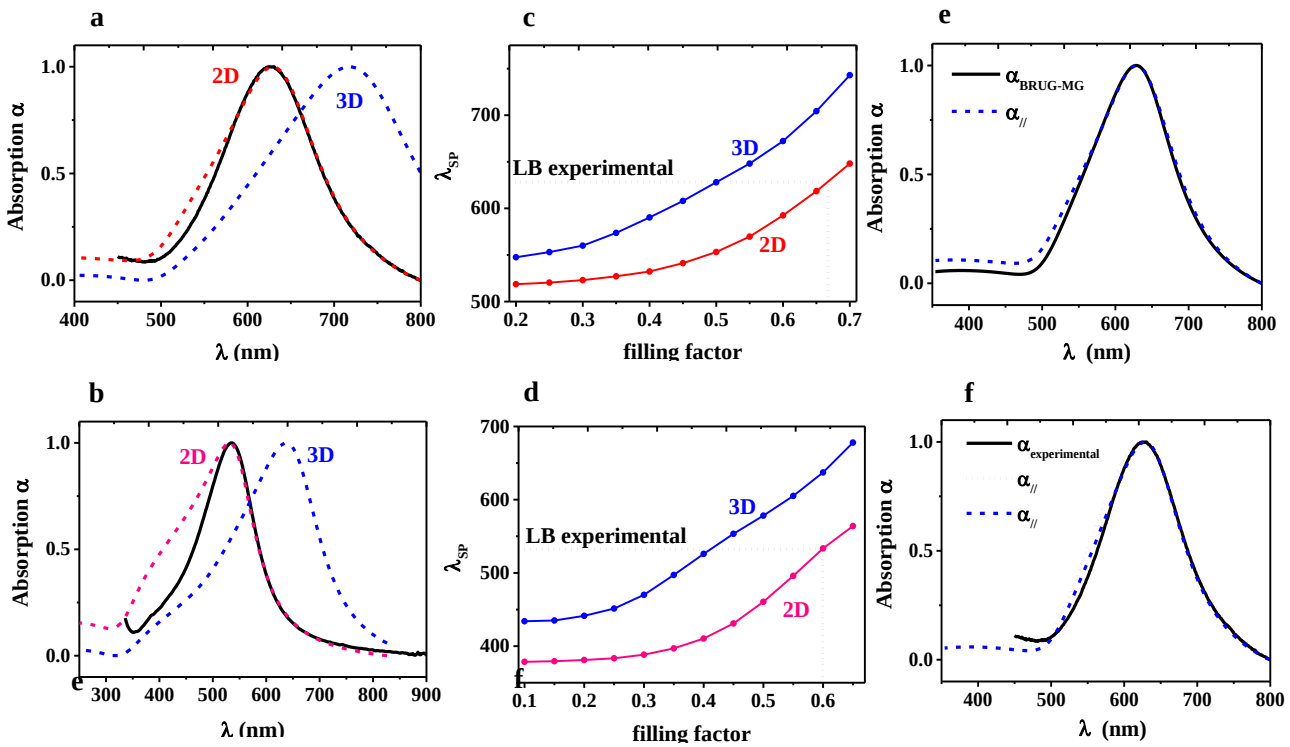

Figure 7. 2D and 3D modelling of surface plasmon with BRUG-MG and image induced dipole models. 7a)-d) position of the surface plasmon resonance λ_{SP} for the 2D and 3D cases with BRUG-MG model, for the Au (figures 7a and 7c) and Ag (figures 7b and 7d). The dotted lines show the experimental positions of the LB monolayers and drop casting films. 7e) Comparison of SP absorption for BRUG-MG (dashed line) and induced dipole (solid line) models for 2D LB monolayer. 7f) SP absorption for the induced dipole model for $\hbar\gamma = 0.18$ (dotted red curve) and 0.06 (dashed blue curve) and experimental 2D LB monolayer (solid black curve).

Effective medium approach including nanoparticle-substrate and nanoparticle-nanoparticle interactions.

An important question then is to know what is the influence of the substrate, particularly in the case of the NPs monolayers. For example it has been shown recently that a blue shift of the SP resonance can be induced[33]. Our approach is to consider the image dipoles on the substrate side induced by NPs as originally developed for metallic islands by Yamagushi *et al.*[14]. The effective dielectric function $\tilde{\varepsilon}_{||}$ parallel to the plane of the substrate is given by:

$$\tilde{\varepsilon}_{||} = \tilde{\varepsilon}_0 \frac{\left[\tilde{\varepsilon}\left(F_{||}+f\right)+\tilde{\varepsilon}_0\left(1-F_{||}-f\right)\right]}{\left[\tilde{\varepsilon}F_{||}+\tilde{\varepsilon}_0\left(1-F_{||}\right)\right]} \qquad (2)$$

where f is the filling factor, $\tilde{\varepsilon}_0$ the dielectric function of the medium surrounding the nanoparticles and $F_{||}$ the depolarizing factor in the direction parallel to the substrate with dielectric function $\tilde{\varepsilon}_s$:

$$F_{\parallel} = A_{\parallel} - \frac{\Gamma^2}{24\eta^2}\frac{\left(\tilde{\varepsilon}_s - \tilde{\varepsilon}_0\right)}{\left(\tilde{\varepsilon}_s + \tilde{\varepsilon}_0\right)} - \frac{\pi^2 d_w}{24a}\frac{2\tilde{\varepsilon}_0}{\left(\tilde{\varepsilon}_s + \tilde{\varepsilon}_0\right)} \qquad (3)$$

$A_{\parallel}$ is the "bare" depolarizing factor of the ellipsoid, i.e. in the absence of the substrate. Γ is the aspect ratio of the ellipsoids (1 in our spherical case), η is the inverse distance of the point dipoles to the substrate normalized by the height of the center of the ellipsoid. d_w is the weight thickness and a is the periodicity of the organized nanoparticles (or average interparticle distance if randomly distributed). The second term of equation (3) corresponds to the image induced contribution by the substrate while the third term is due to the in-plane dipole-dipole interactions between the NPs. Figures 7e) and 7f) represent the fits obtained for the 2D LB monolayers of Au. Fig. 7e) shows the comparison between the SP obtained with the image dipole ($\tilde{\varepsilon}_{\parallel}$) and BRUG-MG ($\tilde{\varepsilon}_{BRUG-MG}$) models. The relevant parameters are the same. It clearly shows the 2D character of the dipolar interactions. The advantage of the image dipole modelling is that the parameters for the NPs are rigorously the same as for the NPs in suspension. For the BRUG-MG it is also the case except for the free electron damping $\hbar\gamma$ which had to be increased by a factor 3 from 0.06 eV to 0.18 eV. As for the bulk $\hbar\gamma = 0.05\ eV$ it shows that the effect of the image induced dipolar interaction is similar to an important broadening of the SP resonance. This is shown in fig. 7e where the two damping parameters have been used in the induced dipole model ($\hbar\gamma = 0.06\ eV$ dashed curve and $\hbar\gamma = 0.18\ eV$ dotted curve) and compared to the experimental 2D LB monolayer (full curve). Let us also stress the relative importance of the array periodicity a and weight thickness d_w.

Conclusion

In conclusion, our approach which combines the surface plasmon analysis of various nanoparticles assemblies and its modelling by Effective Field Medium methods, including realistic interactions with the substrate, show that, even for 10-13 nm sized nanoparticles, dipolar interactions are very large. The effects of dimensionality are highlighted by modelling the spectral position of the surface plasmon resonances of Au and Ag NP monolayers. The models used emphasize the interparticle interactions mediated by their substrate. First it is shown that a combination of Maxwell-Garnett and Bruggeman theories allows taking into account local field effects without overestimating long range mean field dipolar effects. Its predictive character reveals to be powerful. Alternatively, the long range interactions can be minimized by considering the influence of the substrate depolarizing factor on the assemblies of interacting nanoparticles taking into account their mirror images. This is important for applications of two-dimensional nano-devices using monolayers of assembled nanoparticles. We already have indications of such effects for opto-acoustic devices[34] that will be reported elsewhere.

Acknowledgements

J.-Y. B and Y. L. would like to thank the European Research Council for financial support via the ERC Grant "ATOMAG" ERC-2009-AdG-20090325#247452 and the LaBex "Nanoparticles Interacting with their Environment" ANR-11-LABX-0058_NIE.

Notes and references

Institut de Physique et Chimie des Matériaux de Strasbourg, UMR 7504, CNRS, Université de Strasbourg, 23, rue du Loess, BP43, 67034 Strasbourg, France

Electronic Supplementary Information (ESI) available: It contains two sections. Section 1: Synthesis and characterization of silver and gold nanoparticles and Section 2: Modeling of the 2D and 3D nanoparticles optical response.. See DOI: 10.1039/b000000x/

1 J. N. Anker, W. P. Hall, O. Lyandres, N. C.Shah, J. Zhao, R. P. Van Duyne, *Nat. Mat.* 2008, **7**, 442.
2 S. Nie, S. R. Emory, *Science* 1997, **275**, 1102.
3 C. Li, *Nat. Mat.* 2014, **13**, 110.
4 P. K. Jain, I. H. El-Sayed, M. A. El-Sayed, *Nano Today* 2007, **2**, 18.
5 R. Alcaraz de la Osa, , J. M. Sanz, J. M. Saiz, F. González, F. Moreno, *Opt. Lett.* 2012, **37**, 5015.
6 U. Kreibig, M. Vollmer, *Optical Properties of Metal Clusters*. Springer Series in Materials Science, Springer, Berlin, 1995.
7 A. Courty, A.Mermet, P. A. Albouy, E. Duval, M. P. Pileni *Nat. Mat.* 2005, **4**, 395.
8 M. Rycenga, C. M. Cobley, J. Zeng, W.Y. Li, C. H. Moran, Q. Zhang, D. Qin, Y. N. Xia, *Chem. Rev.* 2011, **111**, 3669.
9 E. Hutter, J. H. Fendler, *Adv. Mater.* 2004, **16**, 1685.
10 T. Yamagushi, M. Takigushi, S. Fujioka, H. Takahashi, E. Anno, *Surf. Sci.* 1984, **138**, 449.
11 N. J. Halas, S. Lal, W. S. Chang, S. Link, P. Nordlander, *Chem. Rev.* 2011, **111**, 3913.
12 A. Tao, F. Kim, C. Hess, J. Goldberger, R. R. He, Y. G. Sun, Y.N. Xia, P. D. Yang, *Nano Lett*., 2003, **3**, 1229.
13 D. J. Bergman, *Physics Reports* 1978, **43**, 377.
14 T. Yamagushi, S. Yoshida, A. Kinbara, *Thin Solid Films* 1972, **13**, 261.
15 D. Bedeaux, J. Vlieger, *Physica* 1974, **73**, 287.
16 G. A. Niklasson, H. G. Craighead, *Thin Solid Films* 1985, **125**, 165.
17 K.-H. Su, Q.-H. Wei, X. Zhang, J. J. Mock, D. R. Smith, S. Schultz, *Nano Lett.* 2003, **3**, 1087.
18 B. J. Wiley, S. H. Im, Z.Y. Li, J. McLellan, A. Siekkinen, Y. N. Xia, *J. Phys. Chem.* B 2006, **110**, 15666.
19 P. K. Jain, S. Eustis, M. A. El-Sayed, *J. Phys. Chem. B* 2006, **110**, 18243.
20 S. Lin, M. Li, E. Dujardin, C. Girard, S. Mann, *Adv. Mater*. 2005, 17, 2553.
21 T. R. Jensen, G. C. Schatz, R. P. Van Duyne, *J. Phys. Chem. B* 1999, **103**, 2394.
22 P. K.Jain, W. Huang, M. A. El-Sayed, *Nano Lett.* 2007, **7**, 2080.
23 A. S. Urban, X.Shen, Y. Wang, N. Large, H. Wang, M. W. Knight, P. Nordlander, H. Chen, N. J. Halas, *Nano Lett.* 2013, **13**, 4399.
24 C. Sonnichsen, B. M. Reinhard, J. Liphardt, A. P. Alivisatos, *Nat. Biotech.* 2005, **23**, 741.
25 C. S. Levin , B. G. Janesko , R. Bardhan , G. E. Scuseria , J. D. Hartgerink, N. J. Halas, *Nano Lett.*, 2006, **6**, 2617.
26 M. Pauly, B. P. Pichon, P.-A. Albouy, S. Fleutot, C. Leuvrey, M. Trassin, J.-L. Gallani, S. Begin-Colin, *J. Mater. Chem.* 2011, **21**, 16018.
27 S. Fleutot, G. L. Nealon, M. Pauly, B. P. Pichon, C. Leuvrey, M. Drillon, J.-L. Gallani, D. Guillon, B.Donnio, S. Begin-Colin, *Nanoscale* 2013, **5**, 1507.
28 Shen, Ch.M., Hui, Ch., Yang, T. Z.H., Xiao, C.W., Tian, J.F., Bao, L.Hg., Chen, Sh.T., Ding, H., Gao, H.J. *Chem. Mater.* 2008, **20**, 6939.
29 Q. Zhang, J. Xie, J. Yang, J. Y. Lee, *ACS nano* 2009, **3**, 139.
30 A.Tao, P. Sinsermsuksakul, P. Yang, *Nat. Nanotech.* 2007, **2**, 435.
31 J. Sun, D. Ma, H. Zhang, X. Liu, X. Han, X. Bao, G. Weinberg, N. Pfänder, D. Su, *J. Am. Chem. Soc.* 2006, **128**, 15756.
32 D.A.G. Bruggeman, *Ann. Physik.* (Leipzig) 1935, **24**, 636.
33 S. Raza, W. Yan, N. Stenger, M. Wubs, N. A. Mortensen, *Optics Express* 2013, **21**, 27344.
34 J. Kim, M. Vomir, J.-Y. Bigot, *Phys. Rev. Lett.* 2012, **109**, 166601.